# Ultrawide Temperature Range Super-Invar Behavior of $R_2(Fe,Co)_{17}$ Materials ($R$ = Rare Earth)

Yili Cao,[1] Kun Lin,[1] Sergii Khmelevskyi,[2] Maxim Avdeev,[3,4] Keith M. Taddei,[5] Qiang Zhang,[5] Qingzhen Huang,[6] Qiang Li,[1] Kenichi Kato,[7] Chiu Chung Tang,[8] Alexandra Gibbs,[9] Chin-Wei Wang,[10] Jinxia Deng,[1] Jun Chen,[1] Hongjie Zhang,[11] and Xianran Xing[1,*]

[1]*Beijing Advanced Innovation Center for Materials Genome Engineering, Institute of Solid State Chemistry, University of Science and Technology Beijing, Beijing 100083, China*
[2]*Research Center for Computational Materials Science and Engineering, Vienna University of Technology, Karlplatz 13, A-1040 Vienna, Austria*
[3]*Australian Nuclear Science and Technology Organisation, Lucas Heights, NSW 2234, Australia*
[4]*School of Chemistry, The University of Sydney, Sydney, NSW 2006, Australia*
[5]*Neutron Scattering Division, Oak Ridge National Laboratory, Oak Ridge, Tennessee 37831, USA*
[6]*NIST Center for Neutron Research, National Institute of Standards and Technology, Gaithersburg, Maryland 20899-6102, USA*
[7]*RIKEN SPring- 8 Center, Hyogo 679-5148, Japan*
[8]*Diamond Light Source Ltd., Didcot OX11 0DE, United Kingdom*
[9]*ISIS Neutron and Muon Source, Science and Technology Facilities Council, Didcot OX11 0QX, United Kingdom*
[10]*Neutron Group, National Synchrotron Radiation Research Center, Hsinchu 30076, Taiwan*
[11]*State Key Laboratory of Rare Earth Resource Utilization, Changchun Institute of Applied Chemistry, Chinese Academy of Sciences, Changchun 130022, China*

(Received 29 January 2021; accepted 23 June 2021; published 30 July 2021)

Super Invar (SIV), i.e., zero thermal expansion of metallic materials underpinned by magnetic ordering, is of great practical merit for a wide range of high precision engineering. However, the relatively narrow temperature window of SIV in most materials restricts its potential applications in many critical fields. Here, we demonstrate the controlled design of thermal expansion in a family of $R_2(Fe,Co)_{17}$ materials ($R$ = rare Earth). We find that adjusting the Fe-Co content tunes the thermal expansion behavior and its optimization leads to a record-wide SIV with good cyclic stability from 3–461 K, almost twice the range of currently known SIV. *In situ* neutron diffraction, Mössbauer spectra and first-principles calculations reveal the 3*d* bonding state transition of the Fe-sublattice favors extra lattice stress upon magnetic ordering. On the other hand, Co content induces a dramatic enhancement of the internal molecular field, which can be manipulated to achieve "ultrawide" SIV over broad temperature, composition and magnetic field windows. These findings pave the way for exploiting thermal-expansion-control engineering and related functional materials.

DOI: 10.1103/PhysRevLett.127.055501

It is generally known that materials expand on heating and contract on cooling by virtue of the anharmonicity of interatomic potentials [1,2]. A broad variety of high-precision technological applications, ranging from metrology devices to aerospace structures to optical instruments, require metallic components with zero thermal expansion (ZTE) [3–5], to prevent the size deformation under rapid and frequent thermal shock. These systems were historically termed "super-invar (SIV)" since the 1930s to describe, and were magnetic alloys which neither expanded nor contracted over a certain temperature range [6–9], and whose average linear coefficient of thermal expansion $\bar{\alpha}_1$ was within $1.0 \times 10^{-6}$ $K^{-1}$ (2 orders of magnitude lower than that of common metals) [10]. The nature of the magnetic transition determines the SIV temperature interval typically restricting it to a relatively narrow range near the magnetic ordering temperature, generally less than 200 K [6,11–13]. Such a characteristic contraindicates many applications for critical devices which serve in environments with much larger temperature fluctuations. Here, we explore insights into the essential 3*d* spin-lattice coupling in a family of $R_2(Fe,Co)_{17}$ materials and reveal its contribution to tunable thermal expansion behaviors, through which unprecedentedly wide SIV with good cyclic stability could be manipulated over broad temperature, composition, and magnetic field windows.

The series of $R_2(Fe,Co)_{17}$ compounds was synthesized by the conventional arc-melting method. No phase transformation was observed in the investigated composition range (see Supplemental Material [14] for details).

 

The $Ho_2(Fe,Co)_{17}$ compounds were studied in detail. A careful structural analysis indicated that all compositions were well indexed by a hexagonal symmetry (space group: $P6_3/mmc$). The (Fe,Co) layers with and without Ho atoms stack alternatively along the $c$ direction. Almost no lattice distortion was found throughout the series owing to the part antisite defects. By performing Rietveld refinements using temperature dependent neutron powder diffraction (NPD) data, all investigated $Ho_2(Fe,Co)_{17}$ compounds were found to have a ferrimagnetic (FIM) structure in which the magnetic moments of Ho and Fe/Co were antiparallel and lie in the basal plane [25]. However, a dramatic increase of the magnetic ordering temperature, i.e., Curie temperature ($T_C$), was found with Co substitutions [Figs. 1(b), 1(b) and Supplemental Material, Fig. S8 [14] ]. For example, the $T_C$ was determined to be near 340, 460, and 590 K for $Ho_2Fe_{17}$, $Ho_2Fe_{16}Co$, and $Ho_2Fe_{15}Co_2$, respectively. Magnetization as a function of applied magnetic field ($M$-$H$) show that increasing Co content also monotonously enhances the saturation magnetization at 4 K (near the ground state) [Fig. 1(c)]. Thus, there is clear evidence that optimizing the Fe-Co content can be an effective way to manipulate the magnetic properties of $Ho_2(Fe,Co)_{17}$ compounds.

The temperature dependences of the $Ho_2(Fe,Co)_{17}$ compounds' unit cell volumes ($V$) are shown in Fig. 2(a) (Supplemental Material, Fig. S9 [14]). Intriguingly, highly distinct thermal expansion behaviors emerge across the $Ho_2(Fe,Co)_{17}$ series. For the parent $Ho_2Fe_{17}$ compound, $V$ exhibits a strong negative thermal expansion (NTE) below 340 K, especially from 250 to 340 K. The average volumetric CTEs ($\bar{\alpha}_V$) for the two ranges (3–250 and 250–340 K) were determined to be $[-8.5(3)\times10^{-6}\ \mathrm{K}^{-1}]$ and $-19.4(2)\times10^{-6}\ \mathrm{K}^{-1}$, respectively. However, the NTE behavior weakens remarkably while the working temperature windows simultaneously extend to higher temperatures upon Co substitution. For instance, the NTE behavior is suppressed for the $Ho_2Fe_{15}Co_2$ compound which instead exhibits a low positive thermal expansion (PTE) behavior, $\bar{\alpha}_V = 7.5(4)\times10^{-6}\ \mathrm{K}^{-1}$, from 3 to 590 K. For the intermediate $Ho_2Fe_{16}Co$ composition $V$ essentially remains constant over a wide temperature range, demonstrating an extraordinary ZTE $\bar{\alpha}_V = 0.5(2)\times10^{-6}\ \mathrm{K}^{-1}$ (3–460 K). The apparent ZTE performance of $Ho_2Fe_{16}Co$ is further confirmed by dilatometry [$\bar{\alpha}_l = 0.07(2)\times10^{-6}\ \mathrm{K}^{-1}$, 100–461 K] [Fig. 1(b)]. The intrinsic and apparent CTEs follow the relationship: $\bar{\alpha}_V \approx 3\bar{\alpha}_l$. In contrast, the $Ho_2Co_{17}$ end member shows a typical PTE behavior [$\bar{\alpha}_V = 31.9(1)\times10^{-6}\ \mathrm{K}^{-1}$, 100–600 K] with no anomaly from 10 to 600 K.

Notably, the comparison of Figs. 1(a) and 2(a) shows that the anomalous thermal expansion only exists for temperatures $T < T_C$, indicating a strong coupling between the magnetic ordering and the thermal expansion. The ZTE temperature range achieved in this work (3–461 K, $\Delta T = 458$ K) is far broader than any previously reported SIV [Table I]. For instance, it is about 3.05 times as wide as that of $Fe_{63}Ni_{32}Co_5$ (218–368 K, $\Delta T = 150$ K) [10],

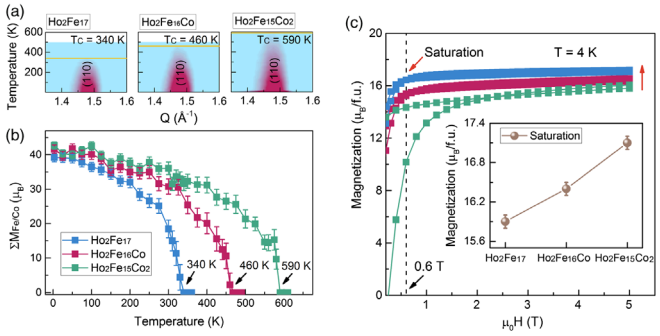


FIG. 1. (a) Contour plot of the neutron powder diffraction (NPD) intensity of magnetic peaks (110) for the three investigated samples: $Ho_2Fe_{17}$, $Ho_2Fe_{16}Co$, and $Ho_2Fe_{15}Co_2$. Yellow line indicates the Curie temperature ($T_C$); (b) temperature dependence of magnetic moments of Fe/Co-sublattice ($\Sigma \boldsymbol{M}_{\mathrm{Fe/Co}}$) determined by NPD refinements; (c) magnetization as a function of applied magnetic field (up to 50 kOe) at 4 K for $Ho_2Fe_{17}$, $Ho_2Fe_{16}Co$, and $Ho_2Fe_{15}Co_2$, respectively. The inset shows the saturation magnetization for these three samples.

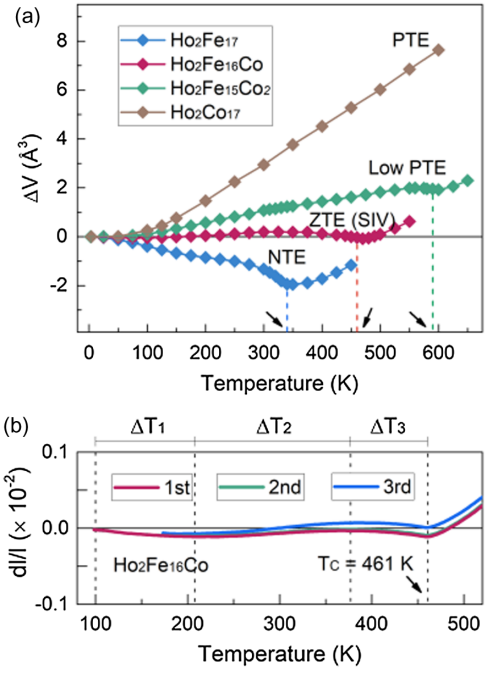


FIG. 2. (a) Temperature dependence of relative unit cell volume determined by NPD refinements from 3 to 650 K for $Ho_2(Fe,Co)_{17}$ compounds; (b) apparent zero thermal expansion of $Ho_2Fe_{16}Co$ compound determined by thermal dilatometer from 100 to 520 K. The coefficients of thermal expansion are further determined within three temperature windows (calculated by using the first measurement): $\bar{\alpha}_l = -0.8(1)\times10^{-6}\ \mathrm{K}^{-1}$, $\Delta T_1 = 100$–$208$ K; $\bar{\alpha}_l = 0.6(0)\times10^{-6}\ \mathrm{K}^{-1}$, $\Delta T_2 = 208$–$377$ K; $\bar{\alpha}_l = -0.9(1)\times10^{-6}\ \mathrm{K}^{-1}$, $\Delta T_3 = 377$–$461$ K, respectively.

TABLE I. Coefficient of thermal expansion CTE and temperature window $\Delta T$ for typical super-invar materials.

| Super-invar materials | Temperature window $\Delta T$ (K) | Coefficient of thermal expansion (CTE, $\times 10^{-6}$ K$^{-1}$) | Reference |
|---|---|---|---|
| $Ho_2Fe_{16}Co$ | 3–461 K ($\Delta T = 458$ K) | $0.07(2) \times 10^{-6}$ K$^{-1}$ ($\alpha_l$) | This work |
| $MnCoGe_{0.99}In_{0.01}$ | 200–310 K ($\Delta T = 110$ K) | $0.68 \times 10^{-6}$ K$^{-1}$ ($\alpha_l$) | [27] |
| $Fe_{63}Ni_{32}Co_5$ | 218–368 K ($\Delta T = 150$ K) | $0.63 \times 10^{-6}$ K$^{-1}$ ($\alpha_l$) | [10] |
| $Zr_{0.8}Nb_{0.2}Fe_2$ | 298–470 K ($\Delta T = 172$ K) | $0.34 \times 10^{-6}$ K$^{-1}$ ($\alpha_l$) | [12,28] |
| $TbCo_{1.9}Fe_{0.1}$ | 123–307 K ($\Delta T = 184$ K) | $0.48 \times 10^{-6}$ K$^{-1}$ ($\alpha_l$) | [13] |
| $Mn_3Cu_{0.5}Ge_{0.5}N$ | 12–230 K ($\Delta T = 218$ K) | $0.12 \times 10^{-6}$ K$^{-1}$ ($\alpha_l$) | [29] |
| $Sc_{0.55}Ti_{0.45}Fe_2$ | 10–250 K ($\Delta T = 240$ K) | $1.24 \times 10^{-6}$ K$^{-1}$ ($\alpha_V$) | [30] |
| $LaFe_{11}Si_2H_x$ | 20–275 K ($\Delta T = 255$ K) | $0.5 \times 10^{-6}$ K$^{-1}$ ($\alpha_l$) | [31] |
| $Gd_{0.25}Dy_{0.75}Co_{1.93}Fe_{0.07}$ | 10–275 K ($\Delta T = 256$ K) | $0.16(0) \times 10^{-6}$ K$^{-1}$ ($\alpha_l$) | [26] |

and 1.72 times as wide as that of $Gd_{0.25}Dy_{0.75}Co_{1.93}Fe_{0.07}$ (10–275 K, $\Delta T = 265$ K) [26]. It is also broader than the ZTE temperature window of other metallic compounds, such as YbGaGe (100–400 K, $\Delta T = 300$ K) in which the ZTE behavior was due to an electronic valence transition [4].

To explore the underlying mechanism behind the magnetic ordering induced anomalous thermal expansion of $Ho_2(Fe,Co)_{17}$ compounds, we performed a detailed first-principles study calculating the electronic structures for a selection of $Ho_2(Fe,Co)_{17}$ compounds in both ferrimagnetically ordered and magnetically disordered [high temperature paramagnetic (PM) phase] states (see Supplemental Material [14] for details). The magnetic disorder in the PM state was modeled using the disordered local moment (DLM) approach [32,33].

Significant differences emerge in the density of states (DOS) upon magnetic ordering. In the DLM state, the bandwidth of the Fe DOS is broad and extends across the Fermi level ($E_F$). In contrast, in the FIM state, the $E_F$ is located near the top of the majority Fe $d$ band [Fig. 3(a) and Supplemental Material, Fig. S11 [14] ]. The almost fully occupied majority band shows a higher local moment for the Fe sublattice. To balance the kinetic energy due to the band splitting, $V$ changes with the increase of local magnetic moment [34]. Intriguingly, it is found that the change in the DOS is mainly attributable to the depopulation of the bonding states in the minority spin channel whereas the nonbonding states increase in the majority spin channel upon magnetic ordering. This implies the weakening of metallic $3d$ bonds upon magnetic ordering and resulting in the expansion of interatomic distance in Fe sublattice (lattice stress derived from magnetic ordering) [11]. It should be noted that for the Co sublattice the increasing population of nonbonding states can be compensated by the depopulation of other nonbonding states in the majority band with increasing spin order [Fig. 3(b) and Supplemental Material, Fig. S11 [14] ]. Accordingly, the lattice stress of the Co sublattice is much smaller and a standard PTE is observed for fully Co-substituted $Ho_2Co_{17}$.

To further test the contribution of the magnetic ordering in the Fe sublattice on the anomalous thermal expansion, the lattice parameters of $Ho_2Fe_{16}Co$ were characterized by isothermal neutron powder diffraction under an external magnetic field (Supplemental Material, Fig. S12 [14]). Here, the same trend discussed previously is observed between the degree of magnetic ordering (as measured by the ordered moment size $|\boldsymbol{M}_{\mathrm{Fe}}|$) and $V$. With increasing magnetic field, both $|\boldsymbol{M}_{\mathrm{Fe}}|$ and $V$ undergo a monotonic enhancement. Notably, the ordered moment saturates at ~0.6 T, which corresponds to the same field above which no further significant change in $V$ is observed [Fig. 3(c)].

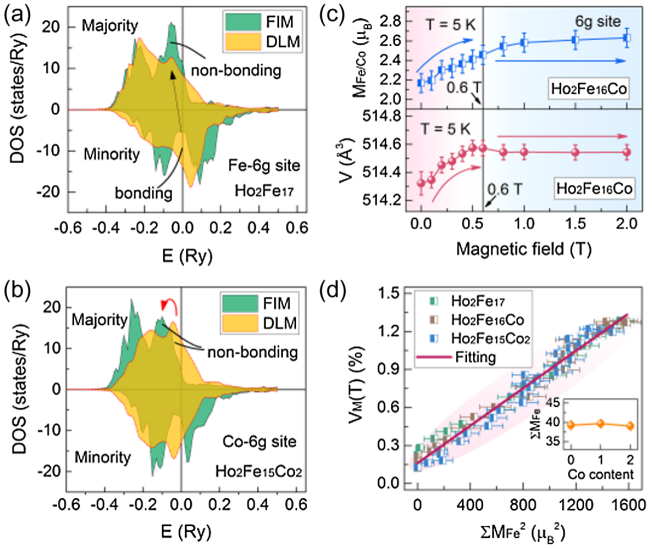


FIG. 3. (a) Atomic resolved contribution to density of state (DOS) of Fe atoms at $6g$ site for $Ho_2Fe_{17}$ compound; (b) Atomic resolved contribution to the DOS of Co atoms at $6g$ sites for $Ho_2Fe_{15}Co_2$ compound; (c) magnetic moments of Fe/Co atoms ($\boldsymbol{M}_{\mathrm{Fe/Co}}$) at $6g$ site and unit cell volume as a function of applied magnetic field for $Ho_2Fe_{16}Co$ compound at 5 K; (d) Positive correlation between the magnetic moments of Fe sublattice ($|\Sigma\boldsymbol{M}_{\mathrm{Fe}}|$) and the contribution of magnetic ordering to the unit cell volume [$V_M(T)$]. The inset shows the $|\Sigma\boldsymbol{M}_{\mathrm{Fe}}|$ as a function of Co content.

Thus, a positive correlation between the magnetic ordering and the lattice volume can be discerned, i.e., a larger $|\boldsymbol{M}_{\mathrm{Fe}}|$ correlates with a larger $V$.

To further quantify this correlation, the unit cell volume $[V_{\mathrm{obs.}}(T)]$ is described by a summation as

$$V_{\mathrm{obs.}}(T) = \mathrm{V}_0 + V_P(T) + V_M(T), \tag{1}$$

where $\mathrm{V}_0$, $V_P(T)$, and $V_M(T)$ are the unit cell volume in ground state and the contribution of phonon and magnetic ordering to the unit cell volume, respectively. Since the $V_M(T)$ is temperature independent above $T_C$, the PTE originates solely from $V_P(T)$ and is well described by the Debye-Grüneisen function $[\alpha_V = dV_P(T)/dT]$ [35]. By subtracting $V_P(T)$ from $V_{\mathrm{obs.}}(T)$, $V_M(T)$ can be isolated below $T_C$ and is seen to increase upon cooling (see Supplemental Material, Fig. S14 [14]). It is found that a large $V_M(T)$ exists and is almost equal for these three samples at 3 K. As the degree of magnetic ordering can be evaluated by the ordered magnetic moments, the positive correlation between $V_M(T)$ and $|\Sigma\boldsymbol{M}_{\mathrm{Fe}}|$ is formulated [Fig. 3(d)]:

$$V_M(T) = k \times |\Sigma\boldsymbol{M}_{\mathrm{Fe}}|^2 + V_{M0}, \tag{2}$$

where $k = 7.4(1) \times 10^{-4}\ \mu_B^{-2}$. It can be seen that at least up to ~12% Co substitution level ($Ho_2Fe_{15}Co_2$) the value of $k$ is still preserved, whose positive value also indicates the $V_M(T)$ is closely proportional to the degree of magnetic ordering of the Fe sublattice, consistent with the results of our DFT calculations.

To shed light on the role of Co in adjusting the thermal expansion, the variation in the magnetic ordering of the Fe sublattice was carefully investigated for $Ho_2(Fe, Co)_{17}$ compounds using $^{57}$Fe Mössbauer spectroscopy performed at 15 K. The distinct magnetic hyperfine splitting shown in Fig. 4(a) (and Supplemental Material [14]) indicates the strong magnetization of the Fe sublattice near the ground state [14]. The analysis of Mössbauer spectra is based on seven sextets assigned to magnetically nonequivalent Fe sites: $4f$, $6g_1$, $6g_2$, $12j_1$, $12j_2$, $12k_1$, $12k_2$ [36]. The similar characteristics of the magnetic hyperfine splitting in our samples imply that the magnetic structure of the Fe sublattice remains almost unchanged for small Co substitution levels, in agreement with the NPD refinements. Intriguingly, the magnitude of the Fe hyperfine field at each crystallographic position increases distinctly with increasing Co content [Fig. 4(b)]. For example, the magnetic hyperfine field of the $4f$ site increases from 36.9(1) T for $Ho_2Fe_{17}$ to 37.9(1) T for $Ho_2Fe_{15}Co_2$ (Supplemental Material, Tables S7–S9 [14]). This suggests that the magnetic exchange interaction in the Fe sublattice is perturbed by Co substitution. By examining the calculated molecular field exchange constants, $J_0$, and the corresponding molecular field acting on the $\boldsymbol{M}_{\mathrm{Fe}}$ (Supplemental Material, Table S10 [14]), it is found that the internal molecular field shows a dramatic enhancement with Co substitution [Fig. 4(c)]. Since the Co atom possesses more $3d$ electrons, the substitutions may promote the Fe band to split below $T_C$ and, consequently, enhance the local magnetization of the Fe sublattice. In this scenario, despite the decreased Fe content, similar $|\Sigma\boldsymbol{M}_{\mathrm{Fe}}|$ and $V_M(T)$ will persist in the ground state for the three samples [inset of Fig. 3(d)].

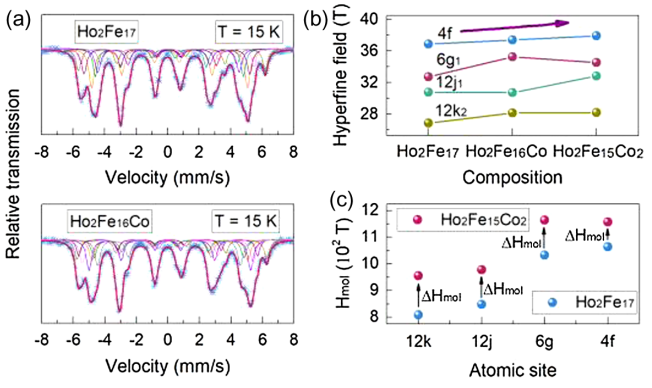


FIG. 4. (a) The $^{57}$Fe Mössbauer spectrum of $Ho_2Fe_{17}$ and $Ho_2Fe_{16}Co$ compounds measured at 15 K; (b) magnetic hyperfine field of Fe atom at each site determined by the Mössbauer spectrum; (c) calculated molecular fields, $H_{\mathrm{mol}}$, acting on $M_{\mathrm{Fe}}$ at each site for $Ho_2Fe_{17}$ and $Ho_2Fe_{15}Co_2$ compounds, respectively.

At the same time, a stronger internal molecular field also suppresses the magnetic disorder derived from thermal fluctuations. Hence, the magnetic ordering of the Fe sublattice becomes more robust to temperature and remains to higher $T_C$. To study this, the rates of change of $|\Sigma\boldsymbol{M}_{\mathrm{Fe}}|(d|\Sigma\boldsymbol{M}_{\mathrm{Fe}}|/dT)$ and unit cell volume $[\mathrm{d}V_{\mathrm{obs.}}(T)/dT]$ were investigated for the three samples. For $Ho_2Fe_{17}$, it is observed that below $T_C$ the $d|\Sigma\boldsymbol{M}_{\mathrm{Fe}}|/dT$ changes rapidly and decreases steeper near $T_C$. This can result in a quick reduction of $V_M(T)$ upon heating $[dV_M(T)/dT]$, and a correspondingly large change in the unit cell volume $[dV_{\mathrm{obs.}}(T)/dT = dV_P(T)/dT + dV_M(T)/dT]$. As the magnitude of $dV_M(T)/dT$ exceeds that of $dV_P(T)/dT$ [i.e., $-dV_P(T)/dT > dV_M(T)/dT$], the NTE behavior will appear in $Ho_2Fe_{17}$ $[dV_{\mathrm{obs.}}(T)/dT < 0]$ (Supplemental Material, Fig. S16 [14]). As Co is introduced, the size of $d|\Sigma\boldsymbol{M}_{\mathrm{Fe}}|/dT$ decreases significantly over the magnetic ordering temperature window. For $Ho_2Fe_{16}Co$ and $Ho_2Fe_{15}Co_2$, $d|\Sigma\boldsymbol{M}_{\mathrm{Fe}}|/dT$ is tuned to a relatively small rate over a wide temperature range [Figs. 5(b) and 5(c)]. In $Ho_2Fe_{16}Co$, $dV_M(T)/dT$ changes gradually and very closely compensates $dV_P(T)/dT$ [i.e., $-dV_M(T)/dT = dV_P(T)/dT$] thereby effecting a nearly temperature independent $V$ over the entire temperature range below $T_C$ [i.e., $dV_{\mathrm{obs.}}(T)/dT = 0$], yielding a form of "ultrawide" SIV. As the Co concentration is further increased (e.g., $Ho_2Fe_{15}Co_2$) the previously carefully balanced magnetic and phonon contributions to the thermal expansion diverge

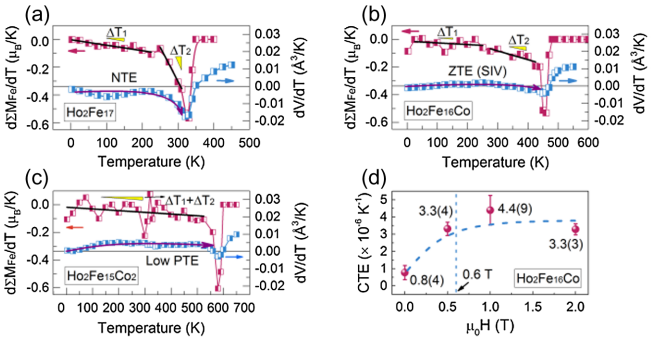


FIG. 5. (a) The rates of the change of $|\Sigma \boldsymbol{M}_{\mathrm{Fe}}|$ ($d|\Sigma \boldsymbol{M}_{\mathrm{Fe}}|/dT$) and unit cell volume ($dV_{\mathrm{obs.}}/dT$) as a function of temperature in $Ho_2Fe_{17}$, (b) $Ho_2Fe_{16}Co$, and (c) $Ho_2Fe_{15}Co_2$ compounds, respectively. (d) The coefficients of thermal expansion (CTEs, 5–250 K) as a function of applied magnetic field from 0 to 2 T for $Ho_2Fe_{16}Co$ compound.

with $-dV_M(T)/dT < dV_P(T)/dT$ leading to a more standard PTE behavior.

To test and expand this design strategy established in $Ho_2(Fe,Co)_{17}$, we studied the thermal expansion properties for $R_2(Fe,Co)_{17}$ compounds with different rare earth elements and tested the efficacy of using an applied magnetic field to tune the internal molecular field. For the former strategy, series of $R_2(Fe,Co)_{17}$ compounds were prepared for $R = Y$, Dy, and Er and the Fe:Co ratio optimized for each $R$ element. In doing so we found a family of wide temperature range SIV systems, with $Y_2Fe_{16.5}Co_{0.5}$ ($\bar{\alpha}_V = 0.2(4) \times 10^{-6}$ K$^{-1}$, 100–400 K), $Dy_2Fe_{16.5}Co_{0.5}$ ($\bar{\alpha}_V = -0.9(5) \times 10^{-6}$ K$^{-1}$, 100–450 K) and $Er_2Fe_{16}Co$ ($\bar{\alpha}_V = -1.7(8) \times 10^{-6}$ K$^{-1}$, 50–375 K) all exhibiting exemplary ZTE properties (Supplemental Material, Fig. S18 [14]). For the latter strategy, the thermal expansion properties of $Ho_2Fe_{16}Co$ were studied under an external magnetic field [Fig. 5(d)]. We found that for the already optimized $Ho_2Fe_{16}Co$ the applied field weakens the SIV properties switching gradually from ZTE to low PTE. Thus, near SIV behavior can be obtained under the magnetic field from 0.5 to 2 T [1 T: $\bar{\alpha}_V = 4.4(9) \times 10^{-6}$ K$^{-1}$; 2 T: $\bar{\alpha}_V = 3.3(3) \times 10^{-6}$ K$^{-1}$] (Supplemental Material, Fig. S20 [14]).

To conclude, a significant insight into the directed design of thermal expansion behaviors was systematically investigated in a family of $R_2(Fe,Co)_{17}$ materials. It revealed that the 3$d$ bonding state transition of the Fe sublattice favors extra lattice stress upon magnetic ordering while the introduction of a little Co induces a strong increase of the internal molecular field, which can be manipulated to extend the magnetic ordering temperature window and tailor the thermal expansion from negative to zero, then to positive smoothly over broad temperature, composition, and magnetic field windows. The record wide SIV temperature range, covering from 3 to 461 K ($\Delta T = 458$ K), is almost twice the value of the known SIVs. Our research together with the flexibility and large number of $R$-Re-Co alloy systems indicates great potential in the development of promising thermal expansion and related functional magnetic performances.

This work was supported by National Natural Science Foundation of China (22090042, 21731001 and 21971009), National Key R&D Program of China (2020YFA0406202). This research used resources of the Advanced Photon Source, a U.S. Department of Energy (DOE) Office of Science User Facility operated for the DOE Office of Science by Argonne National Laboratory under Contract No. DEAC02-06CH11357. The portion of this research used resources at the High Flux Isotope Reactor, a DOE Office of Science User Facility operated by the Oak Ridge National Laboratory.

*Corresponding author.
xing@ustb.edu.cn

[1] J. S. Evans, J. Chem. Soc.-Dalton Trans. **19**, 3317 (1999).
[2] A. L. Goodwin, M. Calleja, M. J. Conterio, M. T. Dove, J. S. Evans, D. A. Keen, L. Peters, and M. G. Tucker, Science **319**, 794 (2008).
[3] P. Mohn, Nature (London) **400**, 18 (1999).
[4] J. R. Salvador, F. Guo, T. Hogan, and M. G. Kanatzidis, Nature (London) **425**, 702 (2003).
[5] E. F. Wassermann, in *Ferromagnetic Materials*, edited by K. H. J. Buschow and E. P. Wohlfarth (North-Holland, Amsterdam, 1990), Vol. 5, p. 237.
[6] S. Chikazumi, J. Appl. Phys. **39**, 939 (1968).
[7] M. Shiga, in *Material Science, and Technology*, edited by R. W. Cahn, P. Haasen, and E. J. Kramer (Weinheim, New York, 1994), Vol. 3B, p. 159.
[8] F. E. Wassermann, J. Magn. Magn. Mater. **100**, 346 (1991).
[9] M. van Schilfgaarde, I. Abrikosov, and B. Johansson, Nature (London) **400**, 46 (1999).
[10] A. Goodwin, G. Halder, C. Kepert, A. Phillips, and K. Chapman, J. Am. Chem. Soc. **132**, 10 (2010).
[11] T. Koshi, Front. Chem. **6**, 267 (2018).
[12] M. Shiga and Y. Nakamura, J. Phys. Soc. Jpn. **47**, 1446 (1979).
[13] Y. Song *et al.*, J. Am. Chem. Soc. **140**, 602 (2018).
[14] See Supplemental Material http://link.aps.org/supplemental/10.1103/PhysRevLett.127.055501 for details of the experimental section, determination of the phase structure, and supporting figures and tables, which includes Refs. [15–24].
[15] M. D. Frontzek, R. Whitfield, K. M. Andrews, A. B. Jones, M. Bobrek, K. Vodopivec, B. C. Chakoumakos, and J. A. Fernandez-Baca, Rev. Sci. Instrum. **89**, 092801 (2018).
[16] S. Calder *et al.*, Rev. Sci. Instrum. **89**, 092701 (2018).
[17] A. V. Ruban and H. L. Skriver, Comput. Mater. Sci. **15**, 119 (1999).
[18] Y. Wang and J. P. Perdew, Phys. Rev. B **44**, 13298 (1991).
[19] E. A. Tereshina, O. Isnard, A. Smekhova, A. V. Andreev, A. Rogalev, and S. Khmelevskyi, Phys. Rev. B **89**, 094420 (2014).
[20] S. Khmelevskyi, A. V. Ruban, Y. Kakehashi, P. Mohn, and B. Johansson, Phys. Rev. B **72**, 064510 (2005).

[21] O. Isnard, D. Hautot, G. J. Long, and F. Grandjean, J. Appl. Phys. **88**, 2750 (2000).
[22] F. Grandjean, O. Isnard, D. Hautot, and G. J. Long, Phys. Rev. B **63**, 014406 (2000).
[23] Y. Cao *et al.*, Inorg. Chem. **59**, 11228 (2020).
[24] L. X. Liao, Z. Altounian, and D. H. Ryan, Phys. Rev. B **47**, 11230 (1993).
[25] P. Álvarez-Alonso *et al.*, Phys. Rev. B **86**, 184411 (2012).
[26] J. Hu *et al.*, Inorg. Chem. **58**, 5401 (2019).
[27] F.-R. Shen *et al.*, APL Mater. **5**, 106102 (2017).
[28] Y. Song, Q. Sun, T. Yokoyama, H. Zhu, Q. Li, R. Huang, Y. Ren, Q. Huang, X. Xing, and J. Chen, J. Phys. Chem. Lett. **11**, 1954 (2020).
[29] X. Song, Z. Sun, Q. Huang, M. Rettenmayr, X. Liu, M. Seyring, G. Li, G. Rao, and F. Yin, Adv. Mater. **23**, 4690 (2011).
[30] Y. Song *et al.*, Mater. Horizons **7**, 275 (2020).
[31] S. Li, R. Huang, Y. Zhao, W. Wang, Y. Han, and L. Li, Adv. Funct. Mater. **27**, 1604195 (2017).
[32] B. L. Gyorffy, A. J. Pindor, J. Staunton, G. M. Stocks, and H. Winter, J. Phys. F **15**, 1337 (1985).
[33] J. Kaspar and D. R. Salahub, Phys. Rev. Lett. **47**, 54 (1981).
[34] S. Khmelevskyi, I. Turek, and P. Mohn, Phys. Rev. Lett. **91**, 037201 (2003).
[35] P. Miao *et al.*, Adv. Mater. **29**, 1605991 (2017).
[36] J. L. Wang, S. J. Campbell, O. Tegus, C. Marquina, and M. R. Ibarra, Phys. Rev. B **75**, 174423 (2007).